Strojniški vestnik - Journal of Mechanical Engineering 53(2007)1, 3-12
UDK - UDC 62-225.5:532.525
Kratki znanstveni prispevek - Short scientific paper (1.03)

Vzporedni vplivi pospeška in površinskega ogrevanja na stisljiv tok: simulacija vesoljske pogonske šobe s srednje veliko površinsko obrabo

Parallel Effects of Acceleration and Surface Heating on Compressible Flow: Simulation of an Aerospace Propulsion Nozzle with a Medium Amount of Surface Wear

A. Alper Ozalp
(Uludag University, Turkey)

Numerične simulacije vesoljskih pogonskih šob so, zaradi nujnosti sočasnega obravnavanja pospeška toka, stopenj prenosa toplote, hrapavosti površine, temperaturno odvisnih lastnosti zraka in sprememb gostote tokovnic zaradi stisljivosti toka, zelo zapletene. Da bi zagotovili pregled za večstransko obravnavo toka pogonskih šob, smo razvili nov računski model, ki vključuje osnosimetrično zveznost, vztrajnostne in energijske enačbe. Izvedli smo računske preizkuse z različnimi geometrijskimi oblikami šob in vstopnimi robnimi pogoji ter s skupno obravnavo površinskega toplotnega toka in hrapavosti. Izračuni so pokazali, da se vstopna moč pogonske šobe in njene izgube povečujejo z večanjem notranjega statičnega tlaka ter zmanjšujejo z zoževalnim kotom šobe in površinskim toplotnim tokom. Ugotovili smo, da je razmerje izgub glede na vstopno moč neodvisno od toplotnega toka, vendar pa se linearno zmanjšuje s povečanjem zoževalnih kotov.

(Ključne besede: pogonske šobe, stisljivi tok, pretočni koeficient, izgube moči)

Numerical simulations of aerospace propulsion nozzles are very complex due to the necessity to simultaneously handle flow acceleration, momentum heat-transfer rates, surface roughness, temperature-dependent air properties and streamwise density variations due to the compressible character of the flow. To provide an overview for a multitask consideration of the propulsion-nozzle flows, a new computational model that integrates the axi-symmetrical continuity, the momentum and the energy equations has been developed. Numerical experiments were performed with various nozzle geometries, inlet-boundary conditions, with the combined handling of the surface heat flux and roughness conditions. The computations indicated that the input and loss power values of the propulsion nozzle increase with higher inlet stagnation pressures and decrease with higher nozzle convergence half angles and surface heat flux. The ratio of the loss to the input power was found to be independent of the heat flux; however, it decreases linearly with an increase in the convergence half angles.

(Keywords: propulsion nozzle, compressible flow, discharge coefficient, power losses)

0 INTRODUCTION

Compressible flows are encountered in a wide variety of engineering applications, e.g., the flow accelerator of environmental control systems in commercial aircraft [1] which supplies fresh air to the passenger cabins of aircraft and the exhaust system of nuclear propulsion engines [2], which generate energy and thrust. Most aerospace applications are equipped with nozzles such that the overall system performance is significantly influenced by the flow acceleration, the surface heating, the inlet conditions and the wear-based friction. Recent studies have pointed out the considerable influence of high pressures and temperatures on the frictional behaviours of nozzle flows. In spite of the objective, an accurate

prediction in the design-oriented calculations of compressible flows is still a challenging task that is becoming increasingly important.

The main design considerations for compressible-flow applications with nozzles are the flow geometries, the inlet-boundary conditions and the flow heat-transfer characteristics, where the performance predictions are reported by several experimental and numerical investigations. The effect of nozzle-exit over-pressure on vortex formation, with its contribution to nozzle thrust, was experimentally examined by Krueger and Gharib [3]. Significant losses in efficiency, due to heat transfer, especially when the ratio of the inlet stagnation to the back pressure converges to unity was determined by Lear et al. [4], who modelled the dissipative effects of heat transfer on the exit kinetic energy and the nozzle efficiency. Orieux et al. [5] illustrated the steady and transient performance of micro-nozzles for various nozzle geometries, ambient conditions and surface cooling, where the thrust values decreased both with cooling and with a narrower nozzle exit. The heat transfer and gas dynamics structure in a choked nozzle with cooling was experimentally investigated by Back et al. [6]. Instabilities in the propulsion of rockets, due to pressure and temperature fluctuations at the upstream of the rocket nozzle and due to the flow geometry, were numerically considered by Assovskii and Rashkovskii [7]. Bartz [8] handled the heat-transfer phenomena in compressible nozzle flows and considered the Nusselt number as a function of the inlet stagnation pressure and the convergence half angle, and Ahmad [9] correlated the variation of the nozzle discharge coefficients and surface heat-transfer values for various nozzle geometries. A 10^{o} convergence half-angle nozzle with different working fluids and with a wide range of inlet stagnation pressures was experimentally considered by Massier et al. [10], who recorded lower discharge coefficients with a decrease in the inlet stagnation pressure. Paik et al. [11] studied the influence of flow geometry and Reynolds number on the variation of the discharge coefficients for sonic nozzles that are applied to gas flow-rate measurements, and reported higher discharge coefficients with an increase in the mass flow rate. Kim et al. [12] considered the effects of several kinds of gases and turbulence models with a wide range of Reynolds numbers on different sonic nozzle geometries. The combined effects of Reynolds number, area ratio and flow velocity on the critical pressure ratio of sonic nozzles were investigated by Park et al. [13]. Sato et al. [14] presented recent data on a real-time air-cooled propulsion ramjet engine. Ribault and Friedrich [15] investigated compressible flow behaviour along adiabatic and cooled walls by implementing the turbulent momentum and heat-transport analogies in a code.

Although the available literature is highly concentrated on heating/cooling applications, inlet/exit conditions and the geometrical structures of the nozzles, surface roughness (ε) is becoming of major interest for compressible/incompressible nozzle flows. Gas-solid particle flows in the nozzles together with the high pressures and temperatures within the flow volume are the main sources of augmentations in the surface roughness. Kumar et al. [16] performed an experimental study of nozzle wear due to gas-solid particle flow and determined an increase in the relative roughness (ε/D_{in}) values from 0.006 to 0.052. Bussiere and Mora [17] presented the real-time data of an Ariane 5 rocket-booster nozzle, where the relative roughness increased from a perfect surface finish to 0.012 during a flight that initiates with a launch and ends with the rocket in orbit.

Although the surface roughness and the surface heat flux act simultaneously in real-time systems, the available literature deals with them separately. The combined effects have not yet been considered. To perform a comprehensive computational study, a new mathematical model, capable of implementing both the surface roughness and the surface heat flux (Q) conditions for aerospace propulsion nozzles was developed. Choked and un-choked cases were investigated for various convergence half angles (α), ratia of inlet stagnation to back pressure ($\beta=(P_o)_{in}/P_b$) and Q cases, and the proposed method was validated with the previous experimental and numerical reports.

1 MODELLING AND COMPUTATION

The overall aim here is to build a predictive model for propulsion-nozzle flows in the presence of surface roughness and constant heat-flux conditions. The model should permit the determination of the necessary design parameters, such as the nozzle geometry and the inlet-boundary conditions for any given performance requirement depending on the applications. Thus, the main requirements are adaptability, simplicity and a short calculation time. The calculations rely on the principles of mass and en-

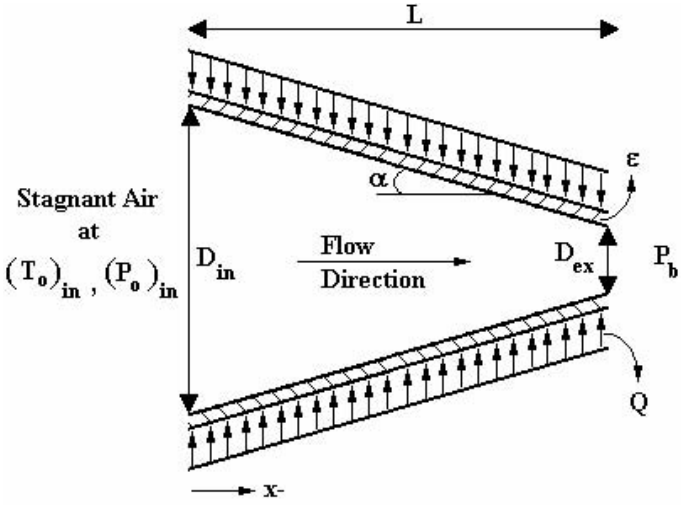

Fig. 1. *Schematic outline of the aerospace propulsion nozzle*

ergy conservation and on the momentum and state equations applied to the control volume, given in Fig. 1. It is assumed that the stagnation conditions of pressure and temperature in the storage tank, upstream of the nozzle, are homogeneous and, as in many numerical studies [2] to [13], the air velocity, pressure and temperature are considered to be uniform across any section normal to the flow axis. Since air properties, like the specific heat at constant pressure (C_p), the kinematic viscosity (ν) and the Prandtl number (Pr), are substantially dependent on temperature (T) [18], they are characterized by 6th-order polynomials with an uncertainty of less than 0.02%, and the temperature dependency is indicated by the superscript T throughout the formulation.

As the study is focused on flows with friction and heat transfer, the stagnation pressure (P_o) and stagnation temperature (T_o) values will also vary in the flow direction with the variation in the Mach number (M). Thus, the conventional equations (Eqs. 1 and 2) for compressible, isentropic and one-dimensional flows are applicable only with the simultaneous handling of the momentum and energy equations.

$$\frac{(P_o)_i}{P_i} = \left(1 + \frac{\gamma - 1}{2} M_i^2\right)^{\frac{\gamma}{\gamma - 1}} \tag{1}$$

$$\frac{(T_o)_i}{T_i} = 1 + \frac{\gamma - 1}{2} M_i^2 \tag{2}$$

$$\dot{m} = \rho_i U_i A_i \tag{3}$$

$$U_i = M_i \sqrt{\gamma R T_i} \tag{4}$$

$$\rho_i = \frac{P_i}{R T_i} \tag{5}$$

$$(\mathrm{Re}_D)_n = \frac{\overline{U_n}\,\overline{D_n}}{\overline{\upsilon_n^T}} \tag{6}$$

The nodal values (subscript i) of the mass flow rate ($\dot{m}$) the air velocity (U) and the density (ρ) can be calculated using Eqs. 3 to 5, where the mass flow rate, the most significant consideration from a numerical point of view, is kept constant in the flow direction. On the other hand, the diameter (D), based the Reynolds number (Eq. 6), is assigned to each differential cell with the mean cellular values of U, D and ν. The friction coefficient (f) is a function of both Re_D and ε (Eq. 7), and the cell-based (subscript n) shear stress (τ) and friction force (F_f) can be expressed with Eqs. 8 to 9.

$$\frac{1}{\sqrt{f_n}} = -3.6 \log\left[\frac{6.9}{(\mathrm{Re}_D)_n} + \left(\frac{\varepsilon / \overline{D_n}}{3.7}\right)^{1.11}\right] \tag{7}$$

$$\tau_n = \overline{f_n}\,\overline{\rho_n}\,\frac{\left(\overline{U_n}\right)^2}{2} \tag{8}$$

$$\left(F_f\right)_n = \tau_n \pi \overline{D_n} \Delta x_n \tag{9}$$

The one-dimensional momentum (Eq. 10) and energy equations (Eq. 11) are applied to each differential cell in the nozzle, where the nodal properties, such as P, U and C_p, are interrelated with the contributions of cellular variants like F_f and the impulse (I). Eq. 11 represents the conservation of mechanical and thermal energy by the implementation of a cell-based surface flux and the frictional loss term.

$$P_i A_i + \dot{m} U_i = P_{i+1} A_{i+1} + \dot{m} U_{i+1} + \left(F_f\right)_n + I_n \tag{10}$$

$$\left(C_P^T\right)_i T_i + \frac{U_i^2}{2} + \frac{Q(A_s)_n}{\dot{m}} = \left(C_P^T\right)_{i+1} T_{i+1} + \frac{U_{i+1}^2}{2} + \frac{\left(F_f\right)_n \overline{U_n}}{\dot{m}} \tag{11}$$

Vargas and Bejan [1] evaluated heat-transfer data in their mathematical model for a compressible nozzle flow, where the Mach number was in the range

0.50 to 0.85, with the empirical correlation of Eq. 12. In the current study the Mach numbers are within 0.05 to 1.0, similar to the subsonic data of [1], and Eq. 12 is applied with the cell-based values of f, Pr and Re_D. Moreover, the combined effects of ε and Q on the mass flow rate are investigated through the non-dimensional discharge coefficient (C_d) of Eq. 13, which compares the real mass flow rate with that of the isentropic case.

$$\left(\mathrm{Nu_D}\right)_n = \frac{\left(\overline{f_n}/2\right)\left[\left(\mathrm{Re_D}\right)_n - 10^3\right]\overline{\mathrm{Pr_n^T}}}{1+12.7\left(\overline{f_n}/2\right)^{0.5}\left[\left(\overline{\mathrm{Pr_n^T}}\right)^{2/3}-1\right]} \qquad (12)$$

$$C_d = \frac{\dot{m}_{real}}{\dot{m}_{isen}} \qquad (13)$$

For the one-dimensional, compressible marching procedure, forward difference discretization is applied in the flow direction, as defined by Chapra and Canale [19]. Since the continuity, momentum and energy equations are to be solved, the geometric domain is divided into n sequential cells, having an equal width equal to Δx. The fineness of the computational grids was examined to ensure that the obtained solutions were independent of the grid employed. Initial runs indicated that with more than 1000 cells the results showed no sign of change with the grid density. Therefore, to provide more reasonable predictions computations were performed with n=1000. Flow parameters, like U, P, T, ρ and stagnation data (P_o, T_o), were calculated at the nodes of these cells, which are numbered from i=1 to n+1, whereas τ, I, Re_D and Nu_D were evaluated on a cell basis using the mean values of nodal inlet and exit data of each cell.

As shown in Fig. 2, by disregarding the surface roughness and heat transfer, the flow of the solution logic first handles the problem as an isentropic type, which is manipulated as described by Laney [20]. The M_{in} value of the isentropic approach is the initial guess of the iterative solution procedure of the non-isentropic nozzle flow. The non-isentropic approach governs the complete equation set described above; however, if the solution scheme encounters singularities, like $M_i>1$, $M_{ex}=1$ & $P_{ex}<P_b$ or $M_{ex}<1$ & $P_{ex}\neq P_b$, M_{in} is modified using a direct Monte Carlo simulation, similar to that explained by Wu and Tseng [21]. The convergence criteria for the mass flow rate throughout the flow volume is of the order of 0.01%, and successive non-isentropic runs were performed until M_{ex} was in the range 0.99 to 1.0 for the choked nozzle, and the shift of P_{ex} from the back pressure is less than $P_b \cdot 10^{-4}$ for the un-choked case.

2 RESULTS AND DISCUSSION

Computations were performed with ratios of the inlet stagnation to the back pressure ($\beta=(P_o)_{in}/P_b$) equal to 1.01, 1.25, 1.50, 1.75 and 2.00, covering both

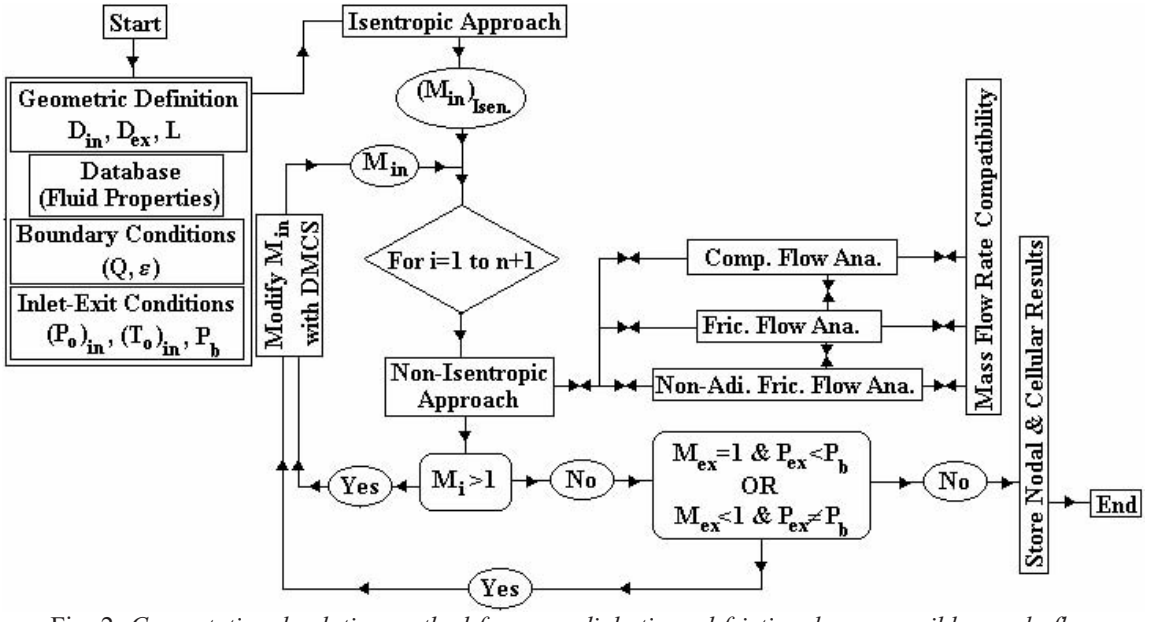

Fig. 2. *Computational solution method for non-adiabatic and frictional compressible nozzle flow*

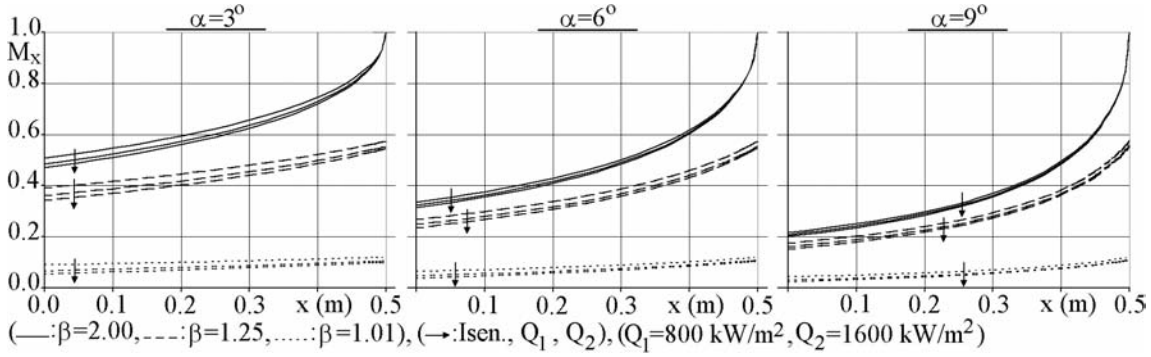

Fig. 3. *Streamwise variation of the Mach number with various α, β and Q conditions*

the un-choked and choked flow cases. To build a comprehensive overview and to include the most frequent geometrical structures, analyses were conducted at nozzle-convergence half angles (α) from 3° to 9°. The medium value of 0.0125, which is similar to the experimental data of Kumar et al. [16] and Bussiere and Mora [17], was selected for the non-dimensional surface roughness (ε/D_{in}) of the nozzle wall, and the effects of constant surface heat flux were evaluated by imposing three distinct values of Q=800, 1200 and 1600 kW/m^2. The results of various design and boundary-condition cases are discussed through streamwise variations of the Mach number, non-dimensional pressure values, flow and surface temperature data and the Nusselt number. Moreover, the influences of the α, β and Q conditions on the discharge coefficient and the input and loss power values are presented for a comparison.

Streamwise Mach-number variations are given in Fig. 3 for various α, β and Q cases. Fig. 3 suggests that flows with a lower β result in a lower M_{in} and M_{ex} for all the nozzle-convergence half angles (α=3° to 9°). When compared with the β=2.00 pattern, β=1.25 caused a decrease of 22.8% and 27.2% in M_{in} for the isentropic and Q=1600 kW/m^2 cases in the α=3° nozzle, whereas the similar ratios for β=1.01 are 82.3% and 88.5%. On the other hand, for the α=9° nozzle, the decreased amounts in M_{in} for β=1.25 were 18.9% and 24.8%, and for β=1.01 they were 80.2% and 85.6% for the isentropic and Q=1600 kW/m^2 cases, respectively. These proportions suggest that the decreased amounts are more apparent for lower α and less for the sharp convergent case (α=9°). In the exit plane the M_{ex} values are identical and equal to 1, being independent of M_{in}, for the β=2.00 case, which corresponds to a choking condition for the complete α range. However, as β is lowered, the nozzles run in the un-choked condition with accompanied decreases in M_{ex}. The variations in M_{ex}, when compared with the above discussions about M_{in}, are small and kept in the range 2 to 4% for the complete α, Q and β set. Fig. 3 further implies that the application of a surface heat flux produces lower M values throughout the nozzle, regardless of the level of β and α. These findings are similar to those of Lear et al.'s [4] numerical and Sato et al.'s [14] experimental determinations. Application of the constant-surface-temperature condition on the nozzle wall [4] caused flow velocities, and thus M, to decrease, whereas the cooling of the nozzle surface [14], which is the opposite operation to that studied here, resulted in higher mass flow rates. For the α=3° nozzle, the heat flux of Q=1600 kW/m^2 results in a decrease in M_{in} by 7.3%, 12.5% and 40% for β equal to 2, 1.25 and 1.01, respectively. On the other hand, the same flux constitutes a lower M_{in} by 6.9%, 11.6% and 36.5% for α=9° in the same β range. These proportions suggest that the effect of the heat flux on the M pattern is more apparent with a lower α.

In compressible flows, static pressure (P) variation is a major consideration since in the case that the inlet stagnation (P_o) values attain significant levels, the nozzle walls will be obliged to face pressure forces that may be at the wear or crack limit of the nozzle material. In fact the conventional theory (Eq. 1) implies that the extreme P value can be as high as P_o, which can be controlled at the nozzle inlet. However, the missing part of the theory is the probability of an augmentation in P_o in the flow direction within the nozzle. Fig. 4 displays the streamwise variation of P, that is non-dimensionalized by the inlet stagnation value of $(P_o)_{in}$. For the complete α range, higher β cases resulted in lower P values at the inlet, which can be attributed to the corresponding higher mass flow rates and inlet Mach numbers, as described in Fig. 3.

On the other hand, with an increase in the surface heat flux, the P values, throughout the flow volume, also increased, which was accompanied by a decrease in the Mach numbers (Fig. 3), and the variations in the static pressures and the Mach numbers were more distinguishable for the nozzles with low convergence half angles (α=3°). For the α=3° case, Fig. 4 further indicates that the pressure values continuously decrease in the streamwise direction if the ratio of the inlet stagnation to the back pressure (β) is kept above 1.25, which is similar to the reports of Kim et al. [12]. This fact keeps the static pressure values below the stagnation value, which in return eliminates the probability of system damage. However, for the lowest β of 1.01, the static pressure values remain around the inlet stagnation value, which is remarkable from the point of view of momentum transfer. In the cases with higher convergence half angles (α=6 to 9°) the local static pressure values exceed the inlet stagnation value by up to 6.3%, particularly for the scenario of α=9°, β=1.01. Simultaneous handling of the momentum and energy equations (Eqs. 10 and 11) suggests that the frictional behaviour of the compressible flow decreases the stagnation pressure in the flow direction; however, the application of the surface heat flux produces the opposite effect on the stagnation pressure. The curves of Fig. 4 indicate that the impact of Q on P_o increases in cases with higher α, where the mass flow rates are comparably smaller. The energy transferred through the nozzle walls is absorbed by the flow, in greater amounts per unit mass for α of 6 to 9° with β=1.01, and stored in stagnation pressure form. As a consequence, increased static pressure values may cause damage to the nozzle structure; moreover, they may also increase the wear rates. The following decrease in P values for x>0.3 m (α=9°) is due to the higher acceleration rates of the flowing air, which can also be seen in Fig. 3.

The streamwise variations of the fluid (T_f) and surface (T_s) temperatures are presented in Fig. 5. As a consequence of the applied surface heat flux, the T_s values are above T_f for the complete α and β ranges and also throughout the flow volume. On the other hand, as the T_s values decrease in the streamwise direction, the opposite is true for T_f in all cases. The decrease rates of T_s become more significant towards the nozzle exit, especially for x>0.45 m, where the highest flow acceleration is determined for all the nozzles. Lower β and higher α indicates lower mass flow rates, which constitutes higher T_s and T_f, especially at the nozzle inlet. The durability of the nozzle material is directly related to the T_s, and the computations suggest the upstream nozzle sections should be carefully considered. On the other hand, surface wear is connected with T_f, and the vital regions appear towards the downstream regions of the nozzle, specifically at the exit plane.

Fig. 6 presents the streamwise variations of surface heat-transfer rates for various convergence-half-angle and pressure-ratio cases, with the application of constant surface heat-flux values of 800 and 1600 kW/m^2. The Nusselt numbers (Nu_D) were observed to increase in the flow direction for the complete set of investigated systems; however, α and Q appeared to cause the Nu_D to decrease in both the choked (β=2.00) and un-choked (β<2.00) cases. This outcome is highly dependent on the fact that narrower nozzles and higher heat-flux values contributed to lower mass flow rate values (Fig. 3), and thus M and U, which also decrease the amount of heat swept from the nozzle wall. On the other hand, the ratio of the exit to inlet Nusselt numbers $\lambda=(Nu_D)_{ex}/(Nu_D)_{in}$ increases with β and α, whereas it decreases with Q. Bartz [8] also reported increased λ ratia with higher α and β; moreover, the typical report of Ahmad [9] for a nozzle with α=45° is λ=3.9. The most significant ratio, evaluated in the present

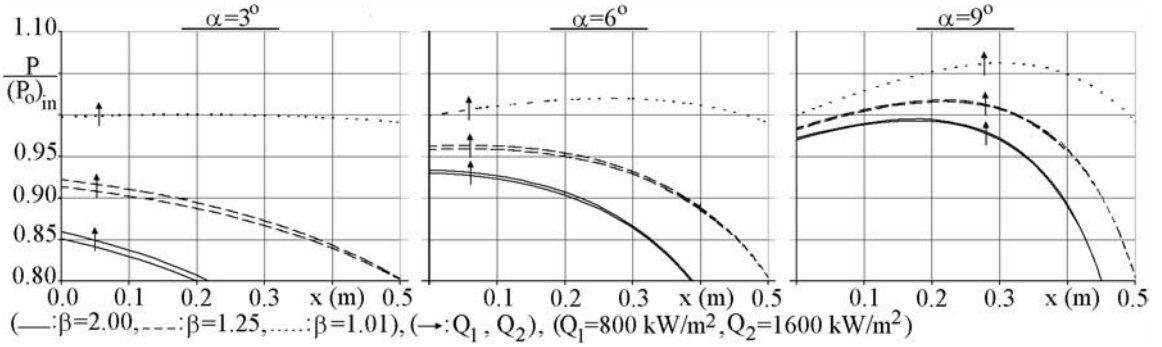

Fig. 4. *Streamwise variation of non-dimensional pressure with various α, β and Q conditions*

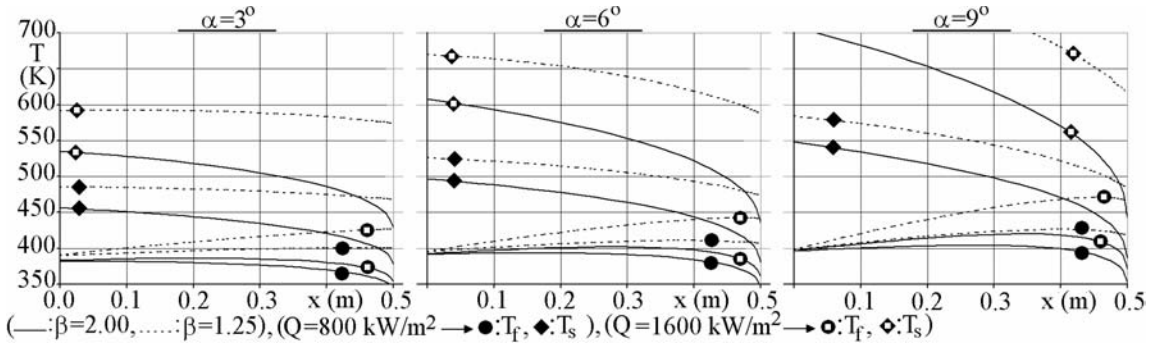

Fig. 5. *Streamwise variation of flow and surface temperature with various α, β and Q conditions*

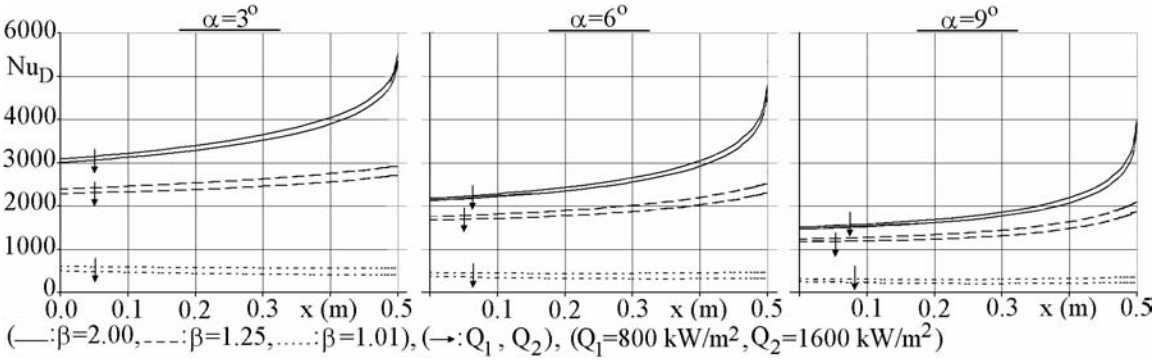

Fig. 6. *Streamwise variation of Nusselt number with various α, β and Q conditions*

paper for the choking case of α=9°, is λ=2.70, and this is higher than the corresponding report of Back et al. [6] (λ=1.61) for the nozzle with α=15°. Fig. 6 further suggests that the application of different heat-flux values causes Nu_D to vary both at the inlet and exit planes of the nozzle. The most significant variations are recorded for the β case of 1.01 for the complete α set, where these intervals are ±9.4% (inlet) and ±19.8% (exit) for α=3° and ±11.8% (inlet) and ±28.1% (exit) for the α=9° case. These values additionally imply that the effect of the wall's heat flux on surface heat-transfer rates becomes more significant in higher α cases, and thus in tasks with lower mass flow rates.

The combined effects of α, Re_D and Q conditions on the discharge coefficient is given in Fig. 7a for the choked case of β=2.00. It can be seen from Fig. 7a that the isentropic values are not only in agreement with the ISO 9300 (Paik et al. [11]) standardized correlation of $C_d=f((Re_D)_{ex})$ for choked nozzles but also with the experimental reports of Massier et al. [10] and Kim et al. [12]. A higher α produced a lower exit Re_D, where the lower Re_D and higher Q are accompanied by reduced values of C_d and point to lower mass flow rates, which show parallelism with the Mach-number variations of Fig. 3 and are similar to the reports of Paik et al. [11].

$$C_d = 0.2636 + 4.6279 \cdot 10^{-2} \ln\left(\mathrm{Re}_D\right)_{ex} \quad (14)$$

$$C_d = \left[1.0106 + 0.0074\left(\ln\alpha\right)^2\right]^{-1} \quad (15)$$

The adiabatic (Q=0) correlations (Eqs. 14 and 15) of Ahmad [9] produce higher C_d values for the present α and Re_D intervals; the gap is the outcome of the applied heat flux values; however, the gap decreases with lower α and with higher $(Re_D)_{ex}$ values. The numerical results show, particularly for the Q=1600 kW/m² case, that the nozzles of α=3°, 6°, 9° result in C_d values of 0.935, 0.933 and 0.93 respectively, where Kim et al. [12] also reported a lower C_d with higher convergence half angles.

The input power (Ψ) necessary to form the compressible flow within the nozzle and the amount of power loss (Ψ_{loss}) are the main considerations from the point of view of the energy requirements to run the propulsion nozzles. Fig. 7(b) demonstrates that both Ψ and Ψ_{loss} increase with higher β and lower α, which indicates that the amount of air directed towards the nozzle is the characteristic design parameter. Increasing the surface heat flux from 800 to 1600 kW/m² caused a decrease in Ψ by 2.7% for all α

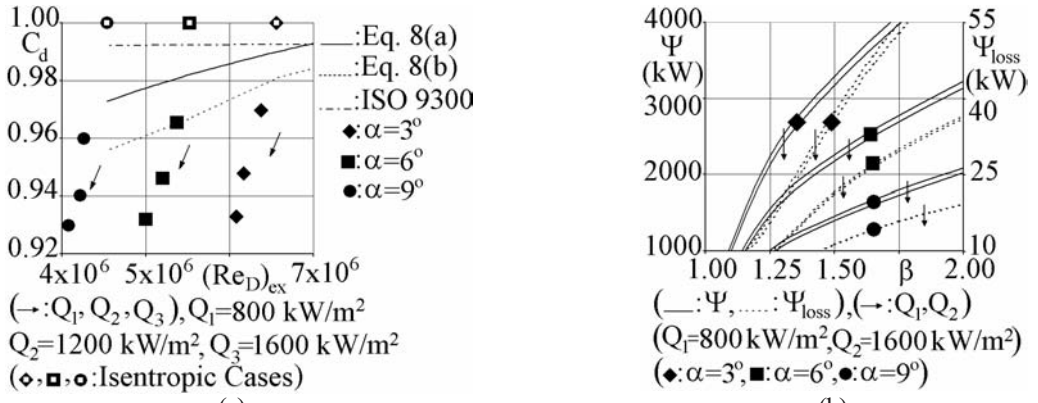

Fig. 7. *Variation of (a) discharge coefficient for the choked flow and (b) input and loss power values with various α, β and Q conditions*

values with β=2.00, where this influence is slightly lower than the C_d gap among the identical cases shown in Fig. 7a. However, the effect of Q on Ψ_{loss} definitely varies with α; as the decrease rate for α=3° is 2.9% the corresponding values for α=6° and α=9° are 1.4% and 0.8%, respectively. Since the main source of Ψ_{loss} is F_f (Eq. 9), Fig. 7b further suggests that Q also has an opposite effect on F_f, which is in agreement with the reports of Ribault and Friedrich [15], who determined higher friction-coefficient values (Eq. 7) with surface cooling. Lastly, the Ψ_{loss}/Ψ ratio is dependent on both α and β and appears to be independent of Q: for β=1.01 the ratio is equal to 0.03% for the complete α set, whereas for β=2.00 the ratio exhibits a linear style and has values of 1.3%, 1.1% and 0.9% for α of 3°, 6° and 9°, respectively.

3 CONCLUSION

A computational method for an investigation of compressible flow and heat-transfer characteristics in aerospace propulsion nozzles was developed. The model is capable of handling various flow geometries and inlet-boundary conditions, together with the simultaneous application of surface heating and roughness conditions. The main conclusions from the numerical experiments can be summarized as follows:

- Surface heating produces lower inlet Mach numbers but higher inlet non-dimensional pressure values; moreover, the effect of Q on both of the values is more apparent in flows with lower acceleration.
- The heat flux, especially in cases with high acceleration, directly increases the stagnation pressure and causes augmented static pressure values, which is remarkable from the point of view of surface wear and system damage, specifically for the nozzle section of 0.25 to 0.40 m. Moreover, the point of maximum shifts downstream in the flows with lower β and a reduced mass flow rate.
- The Nusselt numbers decrease with lower inlet stagnation pressures and with higher convergence half angles and heat-flux conditions; moreover, the effect of surface heat flux on the Nusselt numbers is more apparent in un-choked flows.
- The maximum values of T_s are recorded in the downstream nozzle sections, which is the very important for the nozzle material; and the decrease rates of T_s become significant towards the nozzle exit, especially for x>0.45 m, where the highest flow acceleration is determined for all the nozzle geometries.
- The augmentation of T_f in the flow direction is accompanied by the energy-transfer mechanism and also with the contribution of a lower T_s, and labels the exit-plane neighbourhood as vital from the point of view of wear.

4 NOMENCLATURE

A	cross-sectional area, m²	F_f	frictional force, N
C_d	discharge coefficient	I	thrust, N
C_p	specific heat at constant pressure, J/kgK	L	nozzle length, m
D	nozzle diameter, mm	$\dot{m}$	mass flow rate, kg/s
f	skin friction factor	M	Mach number

Nu_D	Nusselt number
P	pressure, Pa
Pr	Prandtl number
Q	surface heat flux, W/m^2
R	gas constant, J/kgK
Re_D	Reynolds number
T	temperature, K
U	air velocity, m/s
x	streamwise direction, m

Greek Letters

α	convergence half angle, deg
β	ratio of the inlet stagnation to the back pressure
ε	surface roughness, mm
γ	specific heat ratio
ν	kinematic viscosity, m^2/s
ρ	density, kg/m^3
τ	shear stress, Pa
Ψ	power, kW

Subscripts

b, o	back, stagnation
D	diameter
ex, in	exit, inlet
i, n	node, cell number
loss	loss power
s	heat-transfer surface

Superscripts

T	temperature dependency
––	cellular average

5 REFERENCES

[1] Vargas, J.V.C., A. Bejan (2001) Thermodynamic optimization of finned crossflow heat exchangers for aircraft environmental control systems. *Int J Heat Fluid Flow* 22(2001), pp. 657-665.

[2] Kammash, T., T. Godfroy (1997) An open cycle gas core fusion rocket for space exploration. *Acta Astronautica* 41(1997), pp. 229-237.

[3] Krueger, P.S., M. Gharib (2003) The significance of vortex ring formation to the impulse and thrust of a starting jet. *Physics of Fluids* 15(2003), pp. 1271-1281.

[4] Lear, W.E., S.A. Sherif, J.R. Langford (1997) Efficiency and gas dynamics analysis of two-phase mixtures in supersonic nozzles with inter-phase heat transfer and slip. *Acta Astronautica* 40(1997), pp. 701-706.

[5] Orieux, S., C. Rossi, D. Esteve (2002) Compact model based on a lumped parameter approach for the prediction of solid propellant micro-rocket performance. *Sensors and Actuators A-Physical* 101(2002), pp. 383-391.

[6] Back, L.H., P.F. Massier, R.F. Cuffel (1996) Some observations on reduction of turbulent boundary-layer heat transfer in nozzle. *AIAA Journal* 4(1996), pp. 2226-2229.

[7] Assovskii, I.G., S.A. Rashkovskii (2001) Low-frequency instability of solid rocket motors: Influence of the Mach effect and charge geometry. *Combustion, Explosion and Shock Waves* 37(2001), pp. 321-330.

[8] Bartz, D.R. (1957) A simple equation for rapid estimation of rocket nozzle convective heat transfer coefficients. *Jet Propulsion* 27(1957), pp. 49-51.

[9] Ahmad, R.A. (2001) Discharge coefficients and heat transfer for axisymmetric supersonic nozzles. *Heat Transfer Engineering* 22(2001), pp. 40-61.

[10] Massier, P.F., L.H. Back, M.B. Noel, F. Saheli (1970) Viscous effects on the flow coefficient for supersonic nozzle. *AIAA Journal* 8(1970), pp. 605-607.

[11] Paik, J.S., K.A. Park, J.T. Park (2000) Inter-laboratory comparison of sonic nozzles at KRISS. *Flow Measurement and Instrumentation* 11(2000), pp. 339-344.

[12] Kim, H.D., J.H. Kim, K.A. Park, T. Setoguchi, S. Matsuo (2003) Computational study of the gas flow through a critical nozzle. *Proc Instn Mech Engrs Part C: J Mech Eng Sci* 217(2003), pp. 1179-1189.

[13] Park, K.A., Y.M. Choi, H.M. Choi, T.S. Cha, B.H. Yoon (2001) The evaluation of critical pressure ratios of sonic nozzles at low Reynolds numbers. *Flow Measurement and Instrumentation* 12(2001), pp. 37-41.

[14] Sato, T., N. Tanatusgu, Y. Naruo, T. Kashiwagi, J. Omi, J. Tomike, T. Nishino (2000) Development study on ATREX engine. *Acta Astronautica* 47(2000), pp. 799-808.

[15] Ribault, C.L., R. Friedrich (1997) Investigation of transport equations for turbulent heat fluxes in compressible flows. *Int J Heat Mass Trans* 40(1997), pp. 2721-2738.

[16] Kumar, R., A.P. Verma, G.K. Lal (1983) Nozzle wear during the flow of a gas-particle mixture. *Wear* 91(1983), pp. 33-43.
[17] Bussiere, M., B. Mora (1994) Ariane 5 booster nozzle: components description and dimensioning. *Acta Astronautica* 34(1994), pp. 83-89.
[18] Incropera, F.P., D.P. De Witt (1990) Fundamentals of heat and mass transfer. *John Wiley & Sons*, New York.
[19] Chapra, S.C., R.P. Canale (1990) Numerical methods for engineers. *McGraw Hill*, Singapore.
[20] Laney, C.B. (1998) Computational gasdynamics. *Cambridge University Press*, Cambridge.
[21] Wu, J.S., K.C. Tseng (2001) Analysis of micro-scale gas flows with pressure boundaries using direct simulation Monte Carlo method. *Computers and Fluids* 30(2001), pp. 711-735.

Author's Address: Prof. Dr. A. Alper Ozalp
Uludag University
Department of Mechanical Eng.
16059 Gorukle, Bursa, Turkey
aozalp@uludag.edu.tr

Prejeto: 27.4.2005
Received:
Sprejeto: 25.10.2006
Accepted:
Odprto za diskusijo: 1 leto
Open for discussion: 1 year